

Infrared–Infrared Double Resonance Spectroscopy of the Isomers of Acetylene–HCN and Cyanoacetylene–HCN in Helium Nanodroplets[†]

Gary E. Douberly,^{*,‡} Jeremy M. Merritt,[§] and Roger E. Miller^{||}

Department of Chemistry, The University of North Carolina at Chapel Hill,
Chapel Hill, North Carolina 27599-3290

Received: January 2, 2007; In Final Form: March 13, 2007

Infrared–infrared double resonance spectroscopy is used to probe the vibrational dynamics of molecular complexes solvated in helium nanodroplets. We report results for the acetylene–HCN and cyanoacetylene–HCN binary complexes, each having two stable isomers. We find that vibrational excitation of an acetylene–HCN complex results in a population transfer to the other isomer. Photoinduced isomerization is found to be dependent on both the initially excited vibrational mode and the identity of the acetylene–HCN isomer. However, population transfer is not observed for the cyanoacetylene–HCN complexes. The results are rationalized in terms of the *ab initio* intermolecular potential energy surfaces for the two systems with particular emphasis on the long-range barriers to rearrangement.

1. Introduction

Ever since the pioneering work of Scoles¹ and Toennies,^{2,3} 0.4 K helium nanodroplets have proven time and again to be an ideal matrix for many forms of molecular spectroscopy.^{4–8} The remarkable bottom up approach toward cluster formation and rapid cooling provided by the droplets has led to the study of highly metastable^{9–11} and transient^{12–15} species, often at high resolution. Indeed, many examples have illustrated the utility of helium nanodroplets in providing a means to isolate and study molecular species that would have been difficult or impossible to study with conventional gas-phase methods.

Using continuous wave tunable infrared (IR) lasers, the vibrational spectrum in the ground electronic state of many solvated species has been obtained. The vibrational spectrum is acquired by monitoring the helium droplet beam flux as the IR laser is tuned through the vibrational resonances of the molecule. In the vast majority of cases, the excited-state vibrational energy is removed by the droplet, resulting in the evaporation of helium and a corresponding reduction of the droplet beam flux. While there has been extensive work over the past decade to elucidate the mechanisms for the observed rotational and vibrational relaxation, there are still some open questions, including what is the initial fate of a weakly bound hydrogen bonded or van der Waals complex upon vibrational excitation. A recent report on the IR–IR double resonance spectroscopy of the two HCN–HF isomers¹⁶ introduced a technique capable of addressing this question. As discussed below, the data was suggestive of a vibrational relaxation mechanism corresponding to vibrational predissociation of the complex similar to that observed for the linear HCN–HF complex in the gas phase.^{17,18} However, in the helium droplet, a matrix cage effect is observed, which results in the subsequent

recombination of the fragments. As was observed for HCN–HF, if the fragments separate sufficiently within the droplet upon dissociation, an isomerization reaction occurs. While conformational isomerizations have been studied in both rare gas matrices^{19–39} and in the gas phase,^{40,41} the use of helium droplets should prove to be an excellent and universal tool for studying the isomerization dynamics between metastable conformations on a molecular potential energy surface.

Instead of a photoinduced isomerization, it is easy to imagine the first infrared photon initiating a chemical reaction from a weakly bound entrance channel complex. The second, downstream laser in the IR–IR double resonance technique would then be perfectly suited to interrogate the reaction products. In addition, reaction intermediates trapped as result of the rapid cooling available could be probed with various infrared or optical spectroscopic methods. Herein lies the true promise of this and other double resonance helium droplet techniques, that is, the potential to completely characterize the global potential surface from reactants to products. In the current report, we present results on the isomerization dynamics of the HCN–acetylene and HCN–cyanoacetylene binary systems, each having two stable isomers on their respective potential energy surfaces. As shown below, the application of the IR–IR helium droplet double resonance scheme to systems exhibiting differing intermolecular interactions provides further support and insight into the mechanisms responsible for the relaxation of the excited vibrational energy to the helium solvent bath.

2. Experimental Method

The helium droplet apparatus used in the present study has been described in detail elsewhere,⁴² and only a brief description is given here. Helium droplets are formed by expanding high-pressure ultrahigh purity helium gas into vacuum through a 5 μm diameter nozzle, operated at a temperature near 20 K. This expansion produces an approximately log-normal distribution of droplet sizes⁴³ with a mean and half-width determined from published scaling laws^{44,45} for various source conditions. With the nozzle conditions used for the present experiments, droplets are produced with a mean size of approximately 3000 helium

[†] Part of the “Roger E. Miller Memorial Issue”.

* Corresponding author. E-mail: douberly@uga.edu.

[‡] Current address: Department of Chemistry, The University of Georgia, Athens, Georgia 30602.

[§] Current address: Department of Chemistry, Emory University, Atlanta, Georgia 30322.

^{||} Deceased: November 6, 2005.

atoms having a diameter of approximately 6 nm. Complexes of HCN–acetylene or HCN–cyanoacetylene are formed within the droplets as the droplet beam passes through a differentially pumped, 3.5 cm long, gas pick-up cell containing HCN and either acetylene (HCCH) or cyanoacetylene (HCCCN). The partial pressure of HCN in the pick-up cell is optimized such that each droplet on average⁴⁶ “picks up” one HCN molecule. The HCCH or HCCCN gas is then added to the same pick-up cell such that the binary complexes may be formed within the droplets. The translational and internal energy of each monomer along with the condensation energy of the complex is rapidly⁴⁷ removed, resulting in a reduction of the droplet size by approximately 500 helium atoms as the droplet evaporatively cools to a temperature of 0.37 K.²

In a typical IR single resonance experiment, the energy associated with the vibrational excitation of a solvated molecule is quenched by the helium droplet, resulting in the evaporation of approximately an additional 660 helium atoms (5 cm^{-1} per evaporated helium atom).⁴⁷ The IR spectrum of the solvated molecule is recorded by monitoring the laser-induced reduction of the on-axis helium flux, as detected by a bolometer detector, using phase-sensitive techniques (amplitude modulating the IR laser). For the IR–IR double resonance experiments, two spherical mirror laser multipass cells are used to focus multiple passes of the lasers onto the droplet beam to improve the overall sensitivity of the technique. The two multipass cells equipped with Stark electrodes are separated by 8 cm, corresponding to a droplet flight time of approximately $175\ \mu\text{s}$ between the two laser interaction regions. In a previous report on the IR–IR double resonance spectroscopy of the HCCCN monomer in helium droplets,⁴⁸ it was shown that the travel time between the two interaction regions was sufficiently long such that the HCCCN molecules that absorbed a photon from the pump were completely cooled prior to entering the probe laser multipass cell. For the double resonance spectra reported here, the upstream infrared pump is held at a fixed frequency in resonance with a vibrational band of the solvated complex. By amplitude modulating the pump and scanning the unmodulated downstream probe laser, a double resonance spectrum is obtained corresponding to the difference between the infrared spectra of the ground-state complexes obtained with the pump on and off. This double resonance spectrum rides on top of the single resonance signal from the pump. As was recently shown for the two binary isomers of HCN–HF,¹⁶ an enhancement (depletion) in the population of a particular isomer, resulting from photoinduced isomerization, is observed as a positive (negative) signal in the double resonance spectrum.

The probe laser used in the present study is a cw F-center laser (Burleigh FCL-20), operating on crystal no. 3 (RbCl/Li), pumped by 1.5 W of red light from a krypton ion laser (Coherent Sabre). Details of the tuning and calibration of this laser are given elsewhere.⁴⁹ The pump laser is a cw periodically polled lithium niobate optical parametric oscillator (PPLN-OPO) (Linos Photonics). The PPLN crystal is pumped by a single-mode, diode pumped cw YAG laser, yielding a bandwidth of less than 1 MHz. The idler beam has a cw power of approximately 60 mW in the spectral region of interest here, namely 3300 cm^{-1} .

To further improve the pumping efficiency and overall sensitivity, we make use of the pendular-state method,⁵⁰ corresponding to the brute-force orientation of polar solvated complexes using a large dc electric field applied to each laser-droplet beam interaction region. In the present experiments, the polarizations of the infrared laser and OPO were aligned parallel to the static dc electric fields. A factor of 3 improvement in the

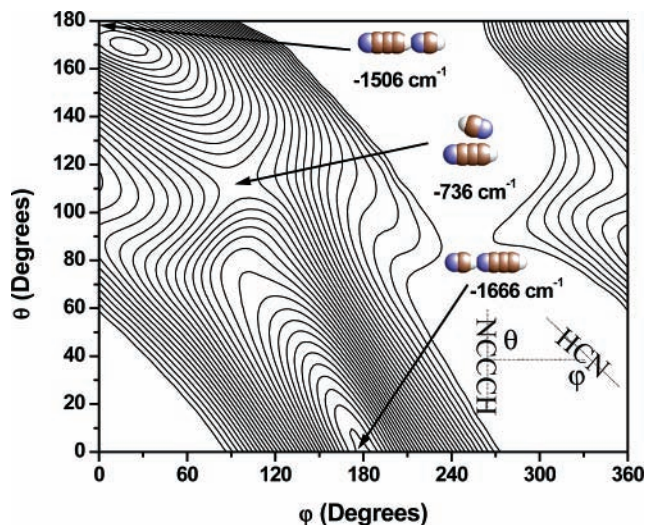


Figure 1. Cut through the potential energy surface (MP2/aug-cc-pVDZ) of the HCN–HCCCN binary system showing minima in both linear geometries. The intermolecular separation between the centers of mass of the two monomers was optimized for each point on the surface. The angles θ and φ correspond to the two in-plane angles, and the contours are separated by 50 cm^{-1} . The values under each graphic correspond to the counterpoise-corrected⁶³ binding energies of each isomer and the transition state obtained from full geometry optimizations at the MP2 level of theory with an aug-cc-pVTZ basis set.⁶⁴

band intensity results from the improved overlap between the laser electric field and the vibrational transition moments of the parallel bands studied here. In addition, for the electric field strengths used here ($\sim 30\text{ kV/cm}$), the rotational structure is collapsed into a single peak at the vibrational band origin,⁵¹ further improving the sensitivity in addition to simplifying the double resonance spectra.

3. Results

3.1. Cyanoacetylene–HCN. Binary molecular complexes having multiple stable isomers within the helium droplets are of interest, as they provide an opportunity to probe photoinduced isomerization dynamics with IR–IR double resonance spectroscopy, as was recently reported for the isomers of HF–HCN.¹⁶ The HCN–HCCCN system is another example of a multi-isomeric system, as is evident from the ground-state electronic intermolecular potential energy surface shown in Figure 1. The counterpoise-corrected ab initio potential surface, calculated at the MP2/aug-cc-pVDZ level of theory, was obtained by fixing the intramolecular degrees of freedom to their equilibrium values for the individual fragments. The intermolecular bond distance, corresponding to the distance between the centers of mass of each fragment, was then optimized at each set of in-plane angles. There are two minima on the potential surface corresponding to the two linear structures and having similar binding energies. Full geometry optimizations and harmonic frequency calculations were performed at a higher level of theory (MP2/aug-cc-pVTZ) for each isomer on the surface along with the transition state between the two, and the results are reported in Table 1.

The more stable HCCCN–HCN isomer ($D_e = -1666\text{ cm}^{-1}$) is separated from the higher energy HCN–HCCCN isomer ($D_e = -1506\text{ cm}^{-1}$) by a 930 cm^{-1} barrier along the minimum energy pathway to isomerization. While the ν_1 and ν_2 spectra of the HCCCN–HCN binary complex have been measured in a molecular beam gas-phase experiment,^{52,53} the higher energy

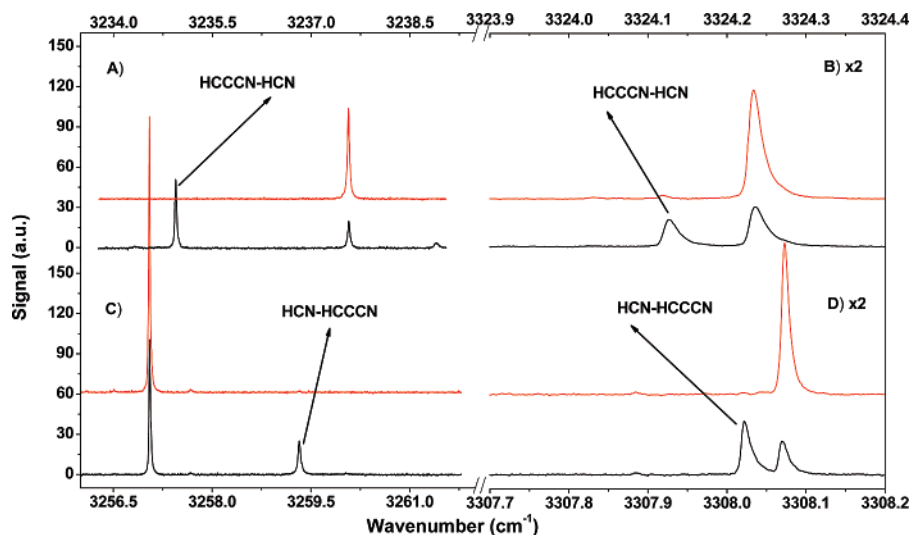


Figure 2. Pendular-state spectra of the HCN–HCCCN isomers recorded at source conditions corresponding to the formation of droplets having a mean size of 3000 atoms. The top spectra in (A) and (D) were recorded with only HCN in the pick-up cell, while the top spectra in (B) and (C) were recorded with only HCCCN present (red). Both HCCCN and HCN were present for the spectrum at the bottom of each set (black). The bands at 3308.07 and 3237.57 cm^{-1} correspond to the C–H stretching vibrations of the HCN dimer, while those at 3324.24 and 3257.12 cm^{-1} are the associated C–H stretch bands of the HCCCN dimer.

TABLE 1: Ab initio Harmonic Frequencies, Dipole Moments, and Counterpoise Corrected Binding Energies⁶³ Obtained at the MP2 Level of Theory with an aug-cc-pVTZ Basis Set

MP2/aug-cc-pVTZ	HCN–HCCH (linear)	HCN–HCCH (T-shaped)	HCN–HCCCN	HCCCN–HCN
ν_0 “free” stretch (cm^{-1})	3455.51	3421.19	3451.38	3466.78
I (km/mol) “free”	79	110	79	87
ν_0 “bonded” stretch (cm^{-1})	3403.34	3409.68	3395.63	3376.10
I (km/mol) “bonded”	270	270	430	490
μ (Debye)	3.62	3.56	7.81	7.93
B'' (cm^{-1})	0.05504	0.06890	0.02355	0.02438
D_e (cm^{-1})	–890	–859	–1506	–1666
transition state (cm^{-1})	–648		–736	

HCN–HCCCN isomer was not observed, presumably due to exchange collisions present in the free-jet expansion that allow the system to condense to the lowest energy configuration. The sequential pick up of fragments into the helium droplets has been shown on several occasions^{9,10,50,54} to result in the formation of exotic species that are difficult or impossible to form in free-jet expansions. The growth of linear chains of $(\text{HCN})_n$ ($n \geq 3$)¹¹ in helium droplets is an example of how long-range intermolecular interactions are important in pre-orienting the complex as the fragments approach one another in the droplet. As the internal energy of each fragment and the condensation energy of the complex are rapidly removed by the helium, the HCN complexes become trapped behind barriers between the locally stable linear complexes and the global minimum cyclic structures. A similar mechanism for the formation of the higher energy HCN–HCCCN complex in helium is likely given the strong long-range dipole–dipole interaction and the significant barrier between the two minima on the HCN–HCCCN potential energy surface.

The pendular-state spectra shown in Figure 2 (lower set, black) were obtained with HCN and HCCCN present simultaneously in a gas pick-up cell with each partial pressure optimized for the pick up of one molecule of each. A large dc field was applied to the downstream (F-center) laser interaction region to collapse the entire rotational structure of each band into one peak near the vibrational band origin. Also shown are the spectra (upper set, red) under the same conditions except either the HCN or the HCCCN was turned off. The top spectra in parts B and C of Figure 2 correspond simply to the free and hydrogen-

bonded C–H stretching bands of the HCCCN dimer, while the top spectra in parts A and D of Figure 2 are the spectra for the HCN dimer. When the two gases are present together in the pick-up cell, four new bands appear that are assigned to the ν_1 and ν_2 bands of the HCN–HCCCN and HCCCN–HCN binary complexes. The new bands that appear in Figure 2A,B are easily assigned to the lower energy HCCCN–HCN C–H stretching bands given their relatively small frequency shifts from the gas-phase band origins. A 0.09 cm^{-1} blue-shift and a 4.06 cm^{-1} red-shift is observed for the “free” and “bonded” C–H stretches, respectively. There are, however, no gas-phase spectra for the HCN–HCCCN complex, but given the small shift from the ν_1 band of the HCN dimer, the band centered at 3308.02 cm^{-1} is assigned to the ν_1 of the HCN–HCCCN isomer, while the band at 3259.33 cm^{-1} is assigned to the ν_2 hydrogen-bonded C–H stretch. Additional support for the assignment of the spectra in Figure 2 comes from the pick-up cell pressure dependence of the pendular bands, indicating that all of the bands correspond to complexes containing a single HCN and HCCCN molecule. The observation of the higher energy HCN–HCCCN isomer is yet another example of how the unique growth processes of clusters in helium droplets allow for the study of novel species that correspond to regions of the intermolecular potential surface far from the global minimum.

We now turn our attention to the IR–IR double resonance spectra of the two isomers of the HCN–HCCCN system. The pump–probe spectra in Figure 3 were recorded by fixing the frequency of the pump to the peak of the pendular band of the vibrational mode indicated along the right side of the figure.

TABLE 2: Constants Obtained from Fitting the HCN–HCCCN Double Resonance Spectra to Two Lorentzians of Opposite Sign^a

pump	probe	$\Delta\nu$	hole		pile		% recovery	pendular γ
			γ	area (au)	γ	area (au)		
$A\nu_1$	$A\nu_1$	0.0083	0.00923	1.70(2)	0.0136	1.60(2)	94 ± 3	0.016
	$B\nu_1$			0		0		
$A\nu_2$	$A\nu_1$	0.0305	0.0156	1.46(2)	0.0427	1.08(3)	74 ± 4	0.049
	$B\nu_1$			0		0		
$B\nu_1$	$A\nu_1$	0.0063	0.00645	0	0.00834	0	98 ± 4	0.012
	$B\nu_1$			1.32(2)		1.29(2)		
$B\nu_2$	$A\nu_1$	0.0299	0.0109	0	0.0750	0	68 ± 4	0.032
	$B\nu_1$			0.642(8)		0.44(2)		

^a Isomer (A) corresponds to HCCCN–HCN, while (B) corresponds to the higher energy HCN–HCCCN isomer. The full width at half-maximum (fwhm) (γ) and the separation between the two Lorentzians ($\Delta\nu$) are in units of cm^{-1} . Also given are the fwhm line widths of the corresponding single resonance pendular spectra of the ν_1 free C–H and the ν_2 bonded C–H stretching bands. The percent recovery corresponds to 100 times the ratio of the pile and hole areas.

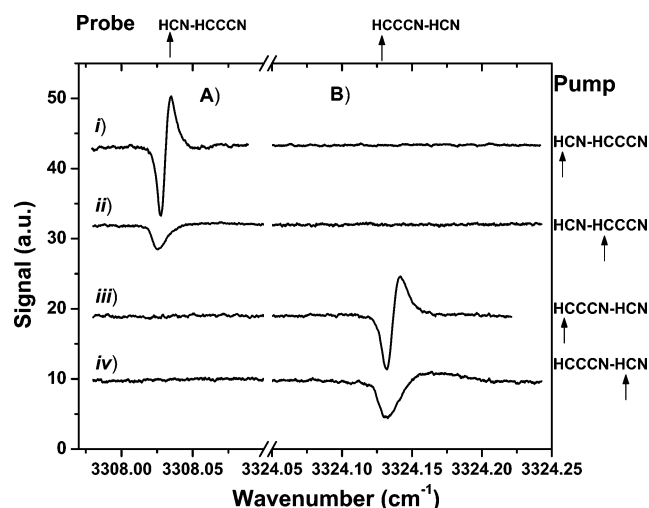


Figure 3. Double resonance spectra of the HCN–HCCCN isomers recorded at source conditions corresponding to a mean droplet size of 3000 helium atoms. For each set of spectra, the probe laser was scanned through the free C–H stretch of both the (A) HCN–HCCCN and (B) HCCCN–HCN isomers, while the pump laser was held at a fixed frequency corresponding to the peak in the pendular spectrum of the (i) HCN–HCCCN free stretch, (ii) HCN–HCCCN bonded stretch, (iii) HCCCN–HCN free stretch, and (iv) HCCCN–HCN bonded stretch.

While amplitude modulating the pump, the probe laser was scanned over the pendular transition region for the free C–H stretch of each isomer, as indicated along the top of the figure. As a result, the signal from the probe laser rides on top of the constant background signal from the pump. In a previous IR–IR double resonance study of the isomers of HCN–HF,¹⁶ we found that excitation of the H–F or C–H stretching vibrations resulted in a population transfer between the isomers. The spectral signature of the population transfer was a net negative double resonance signal for the pumped isomer, while a positive signal was observed downstream for the other isomer that had not been initially excited. Regardless of the vibrational band excited or the identity of the pumped isomer, this spectral signature is missing in the double resonance spectra of HCN–HCCCN, the implication being that, unlike the HCN–HF system, population transfer is not occurring between the two isomers reported here. This is despite the fact that vibrational excitation puts the complex 2400 cm^{-1} above the isomerization barrier. Instead, when the downstream probe laser is scanned through the free C–H stretching band of the pumped isomer, we find a double resonance spectrum having a “hole”, “pile” structure. This is similar to what was previously observed for the HCCCN molecule in helium droplets,⁴⁸ a system that cannot

undergo rearrangement upon vibrational excitation. Upon vibrational excitation, even though the complex does not isomerize, the helium droplet quenches the vibrational energy and the pumped complexes are shifted into a smaller droplet size. As a consequence of this reduction in droplet size, the pendular spectrum of the pumped species shifts to the blue, as was described in detail previously.⁴⁸ The hole and pile features in Figure 3 can then be interpreted as the reduction in population of the pumped isomer in one droplet size, along with an increase in another, approximately 660 helium atoms smaller.

It is important to point out that, in parts A(i) and B(iii) of Figure 3, the double resonance spectra have symmetric hole and pile features, having similar areas when fitted to two Lorentzians of opposite sign (Table 2). In fact, about 98% of the intensity of the hole is accounted for by the intensity of the pile. This is another clear indication that none of the pumped complexes have undergone isomerization. Instead, the excited complexes have simply cooled to the ground state before entering the probe laser region. It is interesting to note that only 70–75% of the intensity of the hole is accounted for when pumping the bonded stretches, as shown in Table 2. This is despite the fact that there is no evidence for population transfer to the other isomer. Additionally, the double resonance spectra are broader than when pumping either of the free stretches. This is interesting given that the same free stretch vibrational modes are being probed in each case, suggesting that the excited population does not lose all memory of the pump process.

In our previous study of HCCCN in helium droplets,⁴⁸ we found that the pendular spectra were inhomogeneously broadened as a result of the distribution of sizes in the droplet beam. As a result of the pump burning a hole in the inhomogeneous profile, the line width of the hole in the HCCCN double resonance spectrum was narrower than the single resonance pendular spectrum. The same is true when pumping the free C–H stretches of the isomers of HCN–HCCCN, which gives holes that have approximately half the width of the single resonance pendular spectra measured with the same nozzle conditions. This is not the case when the pump is resonant with one of the bonded stretches. We find instead that, when probing the free stretches, a hole width is obtained that is the same as the width of the corresponding free stretch single resonance pendular spectrum. In addition, the piles are much broader and shifted to the blue, suggesting a smaller average droplet size upon entering the probe interaction region. It is important to note that the pendular spectra of the bonded stretches appear to be homogeneously broadened, with a fwhm line width that is comparable to the spread of frequencies due to the droplet size distribution. As a result, more of the droplets containing HCN–

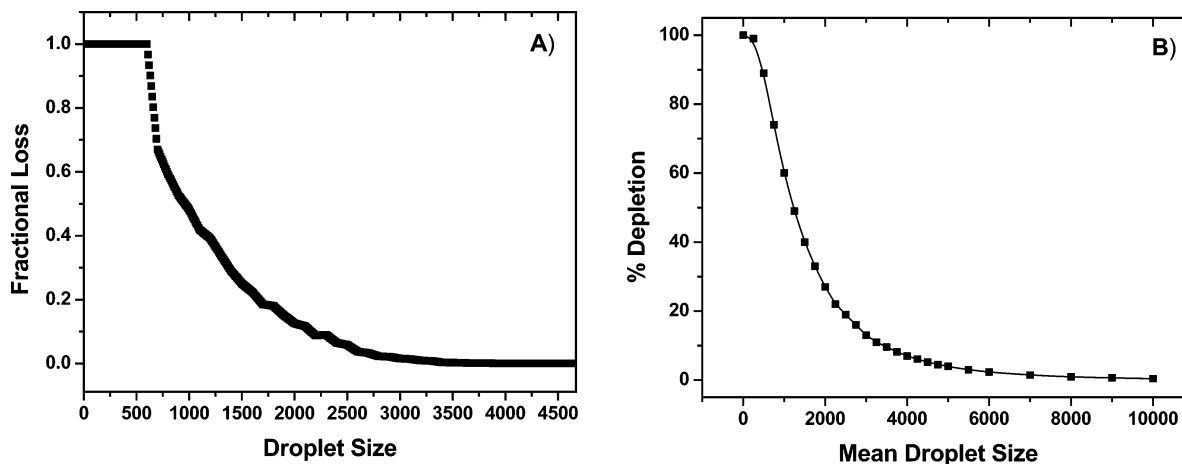


Figure 4. (A) Fraction of droplets that miss the downstream, probe laser interaction region as a result of beam deflection after absorbing a photon in the upstream laser interaction region. The fractional loss approaches one as the droplet size approaches 660 atoms. (B) Percent of the entire pump resonant upstream population that misses the downstream probe laser as a function of the mean droplet size, assuming that the homogeneous line broadening is larger than the inhomogeneous broadening resulting from the log-normal droplet size distribution.

HCCN complexes are in resonance with the pump when the frequency is fixed to the peak of the bonded C–H stretch pendular spectrum. Therefore, the pump does not burn a hole in the droplet size distribution, and the free C–H stretch double resonance hole has the same width as the corresponding single resonance pendular band. While this may explain the different widths observed for the spectra obtained while scanning the probe laser through the free stretch region, we still have not accounted for the 25–30% missing population.

We estimate⁴⁸ that, for the current experimental geometry and a droplet size of 2500 helium atoms, approximately 4% of the droplets will miss the probe laser interaction region. This results from recoil as the droplet cools the initially excited vibrational energy, losing about 660 helium atoms. The agreement between this estimate and what is observed for pumping the free C–H stretches is good although poor for the spectra that correspond to pumping the bonded C–H stretches. However, as mentioned above, the broad holes obtained upon pumping the bonded stretches suggest that more of the droplet distribution contains vibrationally excited complexes. Consequently, we expect that this results in a larger fraction of the droplets being deflected, such that they miss the probe laser. Treating the evaporations as uncorrelated with an energy of 5 cm^{-1} ,⁴⁷ the dependence of the fractional loss on the droplet size is obtained (Figure 4A). While the expected loss is small for a 2500 helium atom droplet (about 5%), the effect becomes much more important as the droplet size decreases. As expected, the fractional loss becomes one as the droplet size approaches 660 helium atoms. Averaging this fractional loss dependence over the log-normal droplet size distributions,⁴³ we obtain the expected percent loss as a function of the initial mean droplet size, as shown in Figure 4B. If the entire droplet distribution is resonant with the pump, a 20% loss of the population as a result of deflection is expected for a mean droplet size of 2500 atoms, the mean size of the droplets used here after considering the losses due to evaporation upon pick-up and complexation of the HCN–HCCN isomers. This value is in reasonable agreement with the experimental results presented in Table 2.

3.2. Acetylene–HCN. In a previous paper from our group,⁵⁵ we reported the helium droplet zero-field rotationally resolved infrared spectra for the linear and T-shaped isomers of HCN–HCCH. While both isomers were also observed in a gas-phase molecular beam experiment,⁵⁶ the relative abundances of the two isomers were found to be considerably different upon cluster

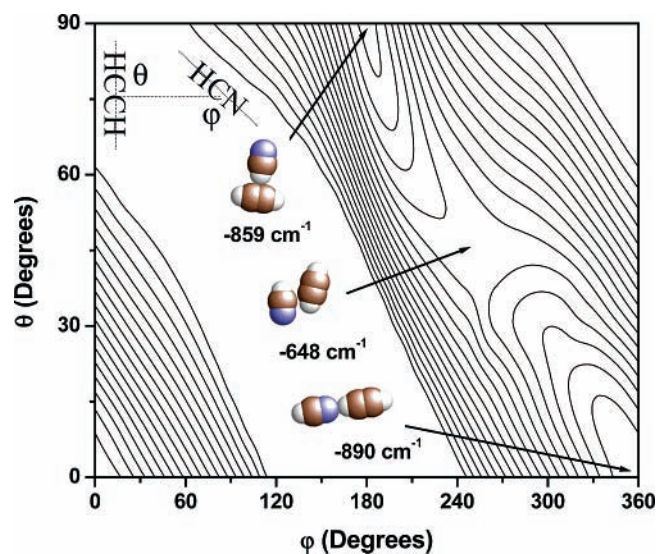


Figure 5. Cut through the potential energy surface (MP2/aug-cc-pVDZ) of the HCN–HCCH binary system showing minima in both the linear and T-shaped geometries. The intermolecular separation between the centers of mass of the two monomers was optimized for each point on the surface. The angles θ and φ correspond to the two in-plane angles, and the contours are separated by 50 cm^{-1} . The values under each graphic correspond to the counterpoise-corrected binding energies of each isomer and the transition state obtained from full geometry optimizations at the MP2/aug-cc-pVTZ level of theory.

formation in helium droplets. From the relative band intensities, we found that the formation of the linear isomer was favored over the T-shaped by a factor of 1.5, whereas the T-shaped isomer was 5.4 times more abundant in the molecular beam. It is still not completely clear why the linear isomer is favored in helium, especially considering that the long-range forces (dipole–quadrupole) would tend to orient the complex into the T-shaped configuration. This suggests instead that the size of the basins on the potential surface that tend to funnel the complex into one well or the other are more important in determining the final isomer formation ratio. A two-dimensional slice of the HCN–HCCH intermolecular potential energy surface is shown in Figure 5. While this *ab initio* surface was produced at the MP2/aug-cc-pVDZ level of theory, the values below each structure are the counterpoise-corrected binding energies using the larger aug-cc-pVTZ basis set. Although the two isomers have similar binding energies, there appears to be

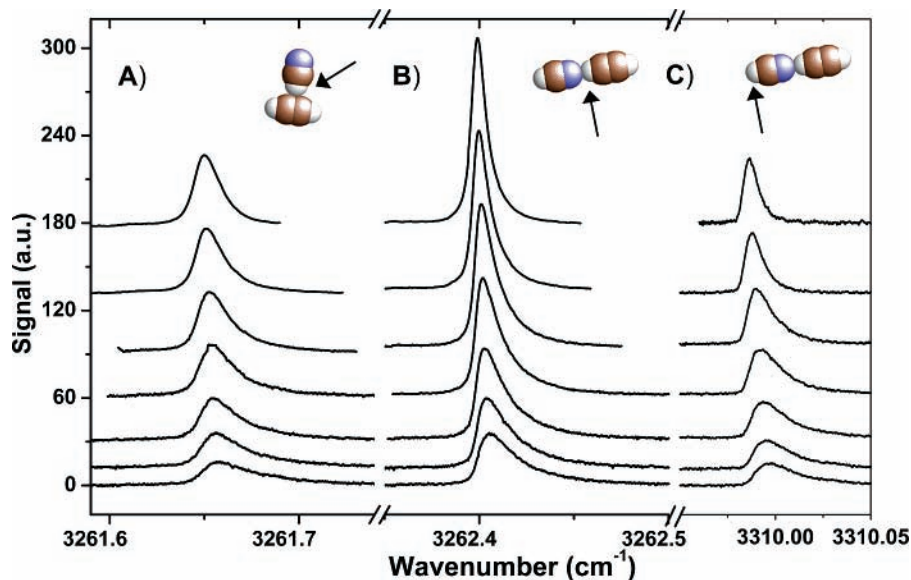


Figure 6. Pendular-state spectra of the HCN–HCCH isomers recorded at various helium droplet source conditions. The mean droplet size ranges from approximately 3000 to 1000 helium atoms, corresponding to a stagnation pressure of 60 atm and a nozzle temperature between 22 and 28 K. The droplet size decreases from top to bottom.

a slightly broader basin leading to the linear well, suggesting that more approach geometries favor the formation of the linear isomer.

The isomerization barrier along the minimum energy path is considerably lower than for the HCN–HCCCN isomers by approximately 600 cm^{-1} . Additionally, the effect of the helium solvent on the size of the potential barriers should be considered. For HCN–HCCCN, the dipole moment undergoes a significant change as the complex moves along the minimum energy path toward the transition state, which corresponds to an antiparallel alignment of the dipoles of HCN and HCCCN. Therefore, the barrier to isomerization for HCN–HCCCN may increase in the helium because the solvation energy is likely larger for the HCN–HCCCN potential minima in comparison to the transition state. In contrast, the HCN–HCCH dipole moment, and presumably the solvation energy, changes much less as the complex moves through the transition state. As a result, the helium solvent may further increase the difference between the isomerization barrier heights for the HCN–HCCCN and HCN–HCCH systems. The calculated barriers suggest that the vibrational dynamics of these two systems will be different, especially considering that vibrational excitation will place the HCN–HCCH complexes about 3100 cm^{-1} above the barrier to rearrangement.

By turning the pump off and tuning the downstream probe laser, we obtain the pendular spectra presented in Figure 6 (HCN and HCCH in the same gas pick-up cell). The bands in Figure 6A,B,C correspond to the hydrogen bonded (HCN) C–H stretch of the T-shaped isomer and the bonded (HCCH, asymmetric) and free (HCN) C–H stretches of the linear isomer, respectively. As previously observed and discussed for HCCCN⁴⁸ in helium droplets, the pendular spectra are asymmetric with a tail to the blue, broadening and shifting to the blue as the mean droplet size decreases. The asymmetric free C–H acetylenic stretch of the T-shaped isomer also lies within the tuning range of our F-center laser, and the zero-field band was previously measured.⁵⁵ When the T-shaped complex is oriented in the strong pendular field, the transition moment of the acetylenic stretch is oriented perpendicular to the laser electric field. With this polarization alignment, the result is a dramatic reduction in the signal intensity. As a result, the double resonance spectra that

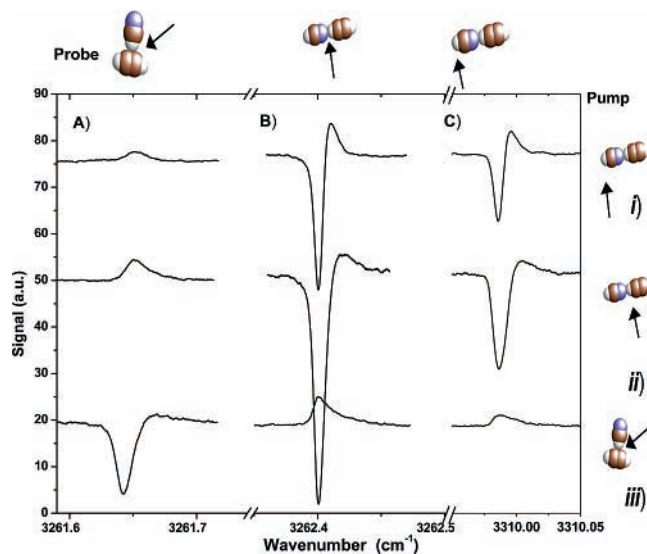


Figure 7. Double resonance spectra of the HCN–HCCH isomers recorded at source conditions corresponding to a mean droplet size of 2500 helium atoms. The sets of spectra (i) and (ii) were recorded with the pump fixed in resonance with the free and the bonded C–H stretching vibrations of the linear isomer, respectively. The spectra in set (iii) correspond to pumping the bonded C–H stretch of the T-shaped isomer. The probe laser was scanned over the (A) T-shaped bonded stretch, (B) linear bonded stretch, and (C) linear free stretch.

correspond to pumping the T-shaped acetylenic stretch were not measured. Additionally, the symmetric C–H acetylenic stretch of the linear isomer is predicted to have very weak IR activity, and this band was not observed.

To record the double resonance spectra for HCN–HCCH, the upstream pump was tuned to the peak of the corresponding pendular spectrum, while the downstream probe laser was scanned over each pendular band to probe for photoinduced isomerization. In Figure 7, the top set of double resonance spectra was obtained when pumping the free C–H stretch of the linear isomer, as indicated along the right side of the figure. The spectra in parts B(i) and C(i) of Figure 7 (probe laser scanned through the C–H stretching bands of the linear isomer) are similar to the double resonance spectra that correspond to

TABLE 3: Constants Obtained from a Fit of the HCN–HCCH Double Resonance Spectra to Two Lorentzians of Opposite Sign^a

pump/probe	$\Delta\nu$ (pile–hole)	hole γ	pile γ	pendular γ
<i>L(H)/L(H)</i>	0.015	0.0094	0.021	<i>L(H)</i> 0.0094
<i>L(H)/L(F)</i>	0.014	0.010	0.027	
<i>L(H)/T(H)</i>			0.020	
<i>L(F)/L(H)</i>	0.0077	0.0078	0.013	<i>L(F)</i> 0.011
<i>L(F)/L(F)</i>	0.0085	0.0079	0.013	
<i>L(F)/T(H)</i>			0.018	
<i>T(H)/L(H)</i>			0.016	<i>T(H)</i> 0.016
<i>T(H)/L(F)</i>			0.021	
<i>T(H)/T(H)</i>	0.022	0.014	0.028	

^a The fwhm (γ) and the separation between the two Lorentzians ($\Delta\nu$) are in units of cm^{-1} . Also given are the fwhm line widths of the corresponding single resonance pendular spectra of the three bands considered here. *L(F)*, *L(H)*, and *T(H)* correspond to the linear free, linear hydrogen-bonded, and T-shaped hydrogen-bonded C–H stretching modes, respectively.

pumping and probing the free C–H stretches of the HCN–HCCCN isomers. The Lorentzian fits, summarized in Table 3, again give hole widths that are each narrower than the single resonance pendular band of the associated probed vibration. Once again, there are piles observed shifted to the blue of the holes. Here the piles correspond to the linear isomer population that has been shifted to the smaller droplet regime as a result of helium evaporation. However, as opposed to the analogous spectra for the isomers of HCN–HCCCN, the holes are deeper than the piles in Figure 7B(i),C(i). Therefore, there appears to be fewer linear isomers downstream when the pump is on rather than when it is off.

To determine if the missing population for the HCN–HCCH linear isomer is due to isomerization, the probe laser was tuned through the bonded C–H stretching band of the T-shaped isomer. Indeed, excitation of the free C–H stretch of the linear isomer results in an increase in the T-shaped population, which leads to a positive double resonance signal, as shown in Figure 7A(i). The efficiency of this photoinduced isomerization is determined by comparing the integrated area of the T-shaped double resonance spectrum (Figure 7A(i)) to the area of the hole obtained from a fit to the linear isomer spectrum (Figure 7C(i)) to two Lorentzians of opposite sign. The results in Table 4 summarize all the areas obtained for the various pump–probe combinations. We find that following vibrational excitation of the linear isomer free stretch, approximately 6% of the pumped complexes are observed downstream as T-shaped isomers. Comparing the positive components of the two double resonance spectra (Figure 7A(i),C(i)), we find that photoinduced isomerization leads to a downstream isomer ratio of 11:1, linear to T-shaped.

When the area from probing the T-shaped isomer is combined with the area of the pile obtained from probing the linear free stretch, the downstream population of linear and T-shaped isomers only accounts for 75% of the initial upstream population that was vibrationally excited by the pump (area of the hole in Figure 7C(i)). While some of the missing population is certainly due to the beam deflection discussed above, the double resonance holes (Figure 7B(i),C(i)) are both narrower than the corresponding single resonance pendular bands, suggesting that linear complexes throughout the entire droplet distribution are not excited, as was the case for the bonded modes of HCN–HCCCN. With regard to the analysis presented in Figure 4A, the percent deflection is predicted to be approximately 5%. Consequently, pumping the free C–H stretch results in an upstream linear population loss (as much as 25%) due to a

channel other than isomerization or beam deflection. One possible channel we considered was the loss of population due to the ejection of a fragment from the droplet following complex dissociation. It is reasonable to suspect that the complex dissociates as it does in the gas phase⁵⁶ because pumping the free stretch results in a vibrationally excited complex 2500 cm^{-1} above the dissociation limit. However, it is unlikely that the translational energy imparted to the fragments upon dissociation^{57–59} would be sufficient to overcome the escape barrier resulting from the helium droplet solvation energy.⁶⁰ Instead, if dissociation occurs, it is more likely that the solvent cages the fragments,⁶¹ leading to recombination on a longer time scale. To test for photoinduced ejection, we tuned the probe laser through the ground-state HCN and HCCH monomer helium droplet spectral region. This test probes specifically for the case where one fragment has been left behind in the droplet and has cooled to the ground state. As for the HCN–HF system,¹⁶ double resonance signals were not observed for either monomer, independent of the pumped mode or the identity of the vibrationally excited isomer, suggesting that ejection is not the source of the missing population. In addition, if a fraction of the excited population has not cooled to the ground state prior to entering the probe interaction region, the vibrationally hot population will be out of resonance with the probe laser, contributing to the missing population. Also, a population loss is expected if the complex dissociates and a fraction of the droplets contain fragments that do not recondense within the flight time between the two laser photolysis volumes. Unfortunately, the results presented here are unable to determine definitively the source of the missing population, and we are left to speculate as to its origin.

The double resonance spectra in Figure 7(ii) were recorded by pumping the acetylenic hydrogen-bonded C–H stretch of the linear HCN–HCCH isomer (*L(H)*). Similarly to pumping the linear free stretch (*L(F)*), a positive double resonance signal is observed when the probe laser is scanned through the T-shaped bonded C–H stretching pendular band (*T(H)*). Once again, we find that vibrational excitation of the linear isomer leads to an increase in the downstream population of T-shaped isomers. However, there are two differences in the sets of double resonance spectra shown in parts (i) and (ii) of Figure 7. Focusing on the percent population recovery in Table 4, we find that, for pumping *L(H)*, only approximately half of the initial upstream population is accounted for in the pile intensities. It is important to point out, however, that the double resonance hole line width (pump/probe *L(H)/L(H)*) is the same as the line width of the single resonance pendular *L(H)* band, in contrast to the line widths for the pump *L(F)* double resonance spectra. This suggests that more population loss results from beam deflection, as discussed above. While the expected deflection differences for pumping *L(F)* and *L(H)* can account for the different percent population recoveries, we still do not have evidence for the source of the additional 25–30% loss observed for all the HCN–HCCH double resonance spectra. Another important difference between the spectra in parts (i) and (ii) of Figure 7 is the linear to T-shaped isomer ratio observed downstream. We find that pumping *L(H)* results in a 3:1 *L:T* downstream isomer ratio. Clearly, photoinduced population transfer from the linear to the T-shaped isomer is most efficient when pumping the hydrogen-bonded C–H stretching mode.

We now turn our attention to the double resonance spectra in Figure 7(iii) obtained with the pump frequency fixed in resonance with the hydrogen-bonded C–H stretch of the T-shaped HCN–HCCH isomer. When the probe laser is tuned

TABLE 4: Areas Obtained by Fitting the Double Resonance Spectra of HCN–HCCH to Two Lorentzians of Opposite Sign Were Corrected for the Different Oscillator Strengths of the Probed Vibrations and the Different Probe Laser Powers^a

pump/probe	corrected hole, pile Lorentz fit areas (au)	% recovery	%(PT) _A	%(PT) _B	L/T ratio	corrected abs int areas (au)
L(H)/L(H)	−2.32(2), 0.73(4)	43 ± 2	12	27	3	−1.34
L(H)/L(F)	−2.22(2), 0.72(2)	45 ± 1	12	27	3	−1.42
L(H)/T(H)						0.27
L(F)/L(H)	−1.25(1), 0.79(2)	72 ± 2	9	12	7	−0.45
L(F)/L(F)	−1.75(2), 1.20(3)	75 ± 2	6	8	11	−0.54
L(F)/T(H)						0.11
T(H)/L(H)						0.42
T(H)/L(F)						0.43
T(H)/T(H)	−1.02(1), 0.32(1)	74 ± 1	42	57	1.3	−0.49

^a The integrated and Lorentzian fit areas were divided by the combined correction factors 1.27, 3.46, and 3.66 for probing the linear free (L(F)), linear hydrogen-bonded (L(H)), and T-shaped hydrogen bonded (T(H)) C–H stretching modes, respectively. The percent recovery is 100 times the ratio of the sum of the positive areas (piles) on both isomers to the negative area (hole) of the pumped isomer. The %(PT)_A corresponds to 100 times the ratio of the downstream linear (T-shaped) population to the upstream T-shaped (linear) population, i.e., the percentage of the total population in resonance with the pump that has undergone photoinduced isomerization and is observed downstream by the probe laser. The %(PT)_B corresponds to the percentage of the total observed downstream population that consists of isomerization products.

through the C–H stretching bands of the linear isomer, positive double resonance signals are observed, indicating that photo-induced isomerization has occurred from the T-shaped to the linear isomer. In fact, of the three vibrational modes of the two isomers, pumping T(H) is the most efficient at shifting the downstream isomer population distribution. Once again, only approximately 75% of the upstream pumped population is excited by the probe laser, as shown above for pumping L(F). Of that 75% of vibrationally excited T-shaped isomers, 57% has isomerized to the linear complex. By comparing the intensity of the positive piles, we find a downstream L:T isomer ratio of 1.3:1 after pumping T(H). Now having compared the three sets of double resonance spectra, it is clear that the isomerization dynamics of the helium-solvated HCN–HCCH complexes are both isomer and mode specific.

4. Discussion

With the helium nanodroplet IR–IR double resonance technique described in the current report, we have demonstrated that, for the HCN–HCCH complexes, vibrational excitation of the C–H stretching modes of one isomer results in a partial population transfer to the other. Additionally, the isomerization dynamics were found to be both strongly mode and isomer specific. We start this section by discussing in detail the differences between the downstream L:T isomer ratios obtained when pumping the L(F), L(H), and T(H) bands of the two HCN–HCCH isomers.

It is interesting to note that we found no evidence for mode specificity in the photoinduced isomerization of the linear HCN–HF isomer to the bent HF–HCN isomer.¹⁶ Instead, pumping both the H–F and C–H stretches led to a downstream isomer ratio of 2:1, linear to bent. In fact, this isomer ratio was equivalent to that observed upon sequential pick-up of each fragment into the droplet. We proposed that this result was at least suggestive of an isomerization mechanism corresponding to vibrational predissociation followed by a solvent caging of the fragments and subsequent recombination of the cold fragments. This mechanism would require that vibrational predissociation occur before the excitation energy is dissipated by the droplet. Additionally, the fragments would have to become sufficiently separated within the droplet such that they lose all memory of their initial relative orientations regardless of whether the C–H or H–F stretch is excited. This seemed plausible given that the well depth of the dipole–dipole interaction of HCN–HF is approximately equal to kT when the fragments are

separated by 4 nm within the droplet. In comparison, the diameter of a 3000 helium atom droplet is about 6.4 nm.

In contrast to the HCN–HF linear isomer, we find that the HCN–HCCH isomerization dynamics are vibrational mode specific. Comparing the pump L(F) and pump L(H) double resonance spectra, we find that population transfer to the T-shaped isomer is approximately three times as efficient if the acetylenic hydrogen-bonded mode is pumped. In addition, neither of the downstream L:T ratios (11:1 pump/probe L(F)/L(F), 3:1 pump/probe L(H)/L(F)) correspond to the ratio observed upon pick-up of the gas-phase molecules, namely 1.5:1. Unlike for HCN–HF, the downstream ratios do not suggest that vibrational excitation leads to sufficiently separated fragments that have completely randomized orientations prior to recondensing. However, we cannot rule out vibrational predissociation as being representative of the early time vibrational dynamics upon absorption of the first infrared photon. Instead, both pumping L(F) and L(H) could lead to dissociation on a time scale that is competitive with helium cooling such that only a fraction of the total population overcomes the barriers to isomerization. The enhanced population transfer observed upon pumping L(H) would then be interpreted as originating from the greater coupling of the acetylenic hydrogen-bonded vibration to the dissociation coordinate in comparison to the free stretch. Pumping L(H), perhaps, leads to fragments that are separated more, on average, in comparison to the fragment separation, if any, produced upon pumping L(F). Certainly, in the gas phase, it was found that the different coupling of the two vibrations to the weak van der Waals bond resulted in mode-specific vibrational predissociation rates with the lifetime of the bonded stretch (1.14 ns) being at least 140 times shorter than the free stretch lifetime.⁵⁶ Of course, we cannot completely rule out the possibility that the weak intermolecular bond never breaks as a result of the solvent cage. Instead, the complex could be internally heated as a result of intramolecular vibrational energy redistribution (IVR),⁶² allowing energy to flow to the isomerization coordinate on a time scale that is competitive with the rate of cooling. Here, the different coupling of the intramolecular C–H stretching vibrations to the lower frequency modes would lead to different IVR rates and therefore influence the downstream L:T isomer ratios.

In addition to the mode specificity observed for the linear isomer, the isomerization efficiencies are also dependent on the identity of the upstream pumped isomer. It is important to note that the lifetimes of the bonded stretch excited states are similar

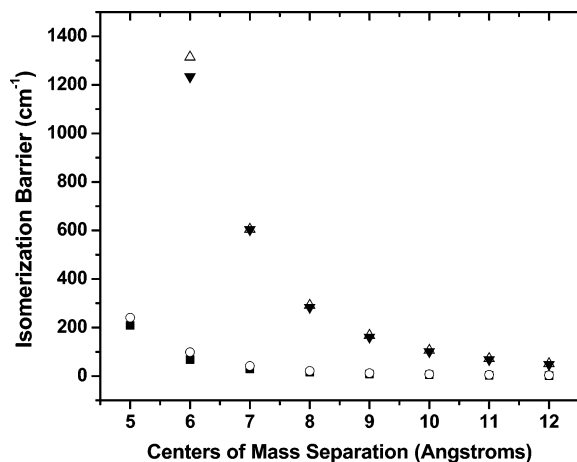


Figure 8. Isomerization barriers for the HCN–HCCH (open circles, solid squares) and HCN–HCCCN complexes (open and solid triangles) at various fixed intermolecular separations. In comparison, the barriers along the minimum energy pathway at the same level of theory (MP2/aug-cc-pVDZ) are 270 and 900 cm^{-1} respectively.

in the gas phase (1.06, 1.14 ns/T-shaped, linear), and the isomerization barriers are essentially the same regardless of the starting geometry. Nevertheless, excitation of the bonded C–H stretching vibrations of the two isomers in helium droplets leads to very different isomerization dynamics. Interestingly, pumping the bonded C–H stretch of the T-shaped isomer does result in a downstream isomer ratio (1.3:1, *L:T*) that is consistent with the ratio observed upon pick-up. In contrast to excitation of the linear isomer, the downstream population ratio here suggests that pumping the bonded stretch of the T-shaped isomer may always lead to cold fragments sufficiently separated within the droplet such that they lose all memory of their initial relative orientations. Subsequent recombination of the cold fragments approaching each other from random initial orientations could then lead to a downstream isomer ratio that is similar to the one observed upon sequential pick-up of the monomer constituents, namely 1.5:1 (*L:T*).

In comparison to the HCN–HCCH isomers, C–H stretch vibrational excitation does not lead to population transfer between the HCN–HCCCN isomers. This is despite the fact that the photon energy is both greater than the isomerization barrier and the dissociation energy. Indeed, in a gas-phase molecular beam,^{52,53} pumping either of the HCCCN–HCN C–H stretches results in vibrational predissociation of the complex. Apparently, the helium droplet either quenches the vibrational energy on a time scale that is fast in comparison to dissociation or the fragments cannot overcome the long-range isomerization barriers after becoming separated within the droplet. While the current experiment cannot differentiate between the two regimes, the latter seems more likely given the vibrational predissociation rates are comparable to those for the HCN–HCCH system in the gas phase,⁵⁶ while the intermolecular interactions at long-range are considerably different.

Ab initio calculations of the barrier to isomerization were carried out for several different fixed intermolecular separations, R , between the HCN and the HCCCN (HCCH) fragments, as shown in Figure 8. The isomerization barrier approaches zero more rapidly for the HCN–HCCH system (solid squares, open circles) than for HCN–HCCCN (solid and open triangles) as the distance between their centers of mass increase. In fact, the isomerization barrier between the two HCN–HCCCN species is greater than 50 cm^{-1} at a 12 Å separation, in contrast to <2 cm^{-1} for HCN–HCCH. At long range, the electrostatic interac-

tion is the main component of the total binding energy. The associated electrostatic interactions are mostly dipole–quadrupole for HCN–HCCH and dipole–dipole for the two polar components of the HCN–HCCCN complexes. Of course, the dipole–quadrupole interaction falls off more rapidly than the dipole–dipole interaction as R increases. Considering the long-range interactions as simply the sum of the dipole–dipole and dipole–quadrupole interactions, we find that the interaction energy in the linear HCN–HCCCN and T-shaped HCN–HCCH orientations is equal to kT (0.26 cm^{-1}) at 68 and 24 Å, respectively. In comparison, the diameter of a 3000 atom helium droplet is approximately 64 Å. If the isomers of HCN–HCCCN undergo vibrational predissociation, the fragments may never sufficiently separate within the droplet to decouple their rotational wavefunctions and randomize their orientations. As a result, vibrational excitation would not lead to population transfer between the isomers. Instead, the long-range dipole–dipole interaction would maintain the relative orientation of the separated fragments, and the monomers would recondense and cool to the ground state of the original well on the potential surface. Certainly, the results reported here for both systems are at least consistent with the proposed vibrational predissociation followed by geminate recombination mechanism. We are hopeful that this work provides a foundation for future time-resolved experimental efforts along with efforts to theoretically model the vibrational and isomerization dynamics of van der Waals complexes solvated in helium droplets.

5. Summary

In summary, IR–IR double resonance spectroscopy was used to probe the isomerization dynamics of the isomers of HCN–acetylene and HCN–cyanoacetylene embedded in liquid helium droplets. For HCN–HCCH, vibrational excitation of either the linear or T-shaped complex resulted in positive double resonance signals on the other isomer, indicating an increase in the downstream population of the isomer not in resonance with the upstream infrared pump. Photoinduced isomerization was observed regardless of the identity of the vibrationally excited isomer. However, the downstream isomer ratios were found to be strongly isomer and vibrational mode specific. Excitation of the hydrogen-bonded C–H stretch of the T-shaped isomer lead to a downstream isomer ratio (1.3 to 1, linear to T-shaped) that was equivalent to the isomer ratio observed upon sequential pick-up by the droplet followed by condensation of the cold subunits. Pumping the bonded C–H acetylenic stretch of the linear isomer lead to a 3 to 1 downstream population ratio in comparison to 11 to 1 upon pumping the linear isomer’s free C–H stretch. The ratios are consistent with vibrational predissociation followed by geminate recombination as the mechanism for isomerization. The rate of dissociation, controlled by the coupling of the intramolecular vibration to the intermolecular dissociation coordinate, apparently plays a critical role in determining the fraction of pumped complexes that become sufficiently separated within the droplet such that they overcome the barriers to isomerization.

In contrast to the isomers of HCN–HCCH, population transfer was not observed between the two linear isomers of HCN–HCCCN. Ab initio calculations of the long-range isomerization barriers show that, in order to randomize the initial relative fragment orientations, a separation of as much as 60 Å must be achieved following vibrational predissociation in comparison to ~20 Å for the isomers of HCN–HCCH. Apparently, the stronger long-range interactions (dipole–dipole)

between the HCN and HCCCN fragments preclude rearrangement between the two linear isomers following vibrational excitation.

Acknowledgment. This work was supported by the National Science Foundation (grant no. CHE-99-87740), and the Air Force Office of Scientific Research (AFOSR). The PPLN-OPO used in this research was acquired with funds from DURIP. G.D. would like to acknowledge the Graduate School at UNC–CH for a Royster Fellowship. We gratefully acknowledge Jochen Küpper for his help in the initial stages of these experiments.

References and Notes

- Goyal, S.; Schutt, D. L.; Scoles, G. *Phys. Rev. Lett.* **1992**, *69*, 933–936.
- Hartmann, M.; Miller, R. E.; Toennies, J. P.; Vilesov, A. F. *Phys. Rev. Lett.* **1995**, *75*, 1566–1569.
- Hartmann, M.; Miller, R. E.; Toennies, J. P.; Vilesov, A. F. *Science* **1996**, *272*, 1631–1634.
- Toennies, J. P.; Vilesov, A. F. *Annu. Rev. Phys. Chem.* **1998**, *49*, 1–41.
- Toennies, J. P.; Vilesov, A. F. *Angew. Chem., Int. Ed.* **2004**, *43*, 2622–2648.
- Choi, M. Y.; Douberly, G. E.; Falconer, T. M.; Lewis, W. K.; Lindsay, C. M.; Merritt, J. M.; Stiles, P. L.; Miller, R. E. *Int. Rev. Phys. Chem.* **2006**, *25*, 15–75.
- Barranco, M.; Guardiola, R.; Hernández, S.; Mayol, R.; Navarro, J.; Pí, M. *J. Low Temp. Phys.* **2006**, *142*, 1–81.
- Stienkemeier, F.; Lehmann, K. K. *J. Phys. B: At., Mol. Opt. Phys.* **2006**, *39*, 127–166.
- Douberly, G. E.; Miller, R. E. *J. Phys. Chem. B* **2003**, *107*, 4500–4507.
- Nauta, K.; Miller, R. E. *Science* **2000**, *287*, 293–295.
- Nauta, K.; Miller, R. E. *Science* **1999**, *283*, 1895–1897.
- Merritt, J. M.; Küpper, J.; Miller, R. E. *Phys. Chem. Chem. Phys.* **2005**, *7*, 67–78.
- Küpper, J.; Merritt, J. M.; Miller, R. E. *J. Chem. Phys.* **2002**, *117*, 647–652.
- Rudic, S.; Merritt, J. M.; Miller, R. E. *J. Chem. Phys.* **2006**, *124*, 104305.
- Merritt, J. M.; Rudic, S.; Miller, R. E. *J. Chem. Phys.* **2006**, *124*, 084301.
- Douberly, G. E.; Merritt, J. M.; Miller, R. E. *Phys. Chem. Chem. Phys.* **2005**, *7*, 463–468.
- Miller, R. E. *Acc. Chem. Res.* **1990**, *23*, 10–16.
- Dayton, D. C.; Miller, R. E. *Chem. Phys. Lett.* **1988**, *143*, 181–185.
- Coussan, S.; Bouteiller, Y.; Perchard, J. P.; Brenner, V.; Millie, P.; Zheng, W. Q.; Talbot, F. *J. Chem. Phys.* **1999**, *110*, 10046–10057.
- Coussan, S.; Loutellier, A.; Perchard, J. P.; Racine, S.; Peremans, A.; Tadjeddine, A.; Zheng, W. Q. *Chem. Phys.* **1997**, *223*, 279.
- Coussan, S.; Bouteiller, Y.; Loutellier, A.; Perchard, J. P.; Racine, S.; Peremans, A.; Zheng, W. Q.; Tadjeddine, A. *Chem. Phys.* **1997**, *219*, 221–234.
- Coussan, S.; Loutellier, A.; Perchard, J. P.; Racine, S.; Peremans, A.; Tadjeddine, A.; Zheng, W. Q. *J. Chem. Phys.* **1997**, *107*, 6526–6540.
- Coussan, S.; Bakkas, N.; Loutellier, A.; Perchard, J. P.; Racine, S. *Chem. Phys. Lett.* **1994**, *217*, 123–130.
- Coussan, S.; Alikhani, M. E.; Perchard, J. P.; Zheng, W. Q. *J. Phys. Chem. A* **2000**, *104*, 5475–5483.
- Coussan, S.; Brenner, V.; Perchard, J. P.; Zheng, W. Q. *J. Chem. Phys.* **2000**, *113*, 8059–8069.
- Heikkilä, A.; Pettersson, M.; Lundell, J.; Khriachtchev, L.; Räsänen, M. *J. Phys. Chem. A* **1999**, *103*, 2945–2951.
- Coussan, S.; Bouteiller, Y.; Perchard, J. P.; Zheng, W. Q. *J. Phys. Chem. A* **1998**, *102*, 5789–5793.
- Roubin, P.; Varin, S.; Verlaque, P.; Coussan, S.; Berset, J. M.; Ortega, J. M.; Peremans, A.; Zheng, W. Q. *J. Chem. Phys.* **1997**, *107*, 7800–7808.
- Pettersson, M.; Maçõas, E. M. S.; Khriachtchev, L.; Fausto, R.; Räsänen, M. *J. Am. Chem. Soc.* **2003**, *125*, 4058–4059.
- Pettersson, M.; Lundell, J.; Khriachtchev, L.; Räsänen, M. *J. Am. Chem. Soc.* **1997**, *119*, 11715–11716.
- Maçõas, E. M. S.; Fausto, R.; Lundell, J.; Pettersson, M.; Khriachtchev, L.; Räsänen, M. *J. Phys. Chem. A* **2000**, *104*, 11725–11732.
- Maçõas, E. M. S.; Khriachtchev, L.; Pettersson, M.; Fausto, R.; Räsänen, M. *J. Am. Chem. Soc.* **2003**, *125*, 16188–16189.
- Maçõas, E. M. S.; Khriachtchev, L.; Pettersson, M.; Lundell, J.; Fausto, R.; Räsänen, M. *Vib. Spectrosc.* **2004**, *34*, 73–82.
- Maçõas, E. M. S.; Khriachtchev, L.; Pettersson, M.; Juselius, J.; Fausto, R.; Räsänen, M. *J. Chem. Phys.* **2003**, *119*, 11765–11772.
- Maçõas, E. M. S.; Khriachtchev, L.; Pettersson, M.; Fausto, R.; Räsänen, M. *J. Chem. Phys.* **2004**, *121*, 1331–1338.
- Maçõas, E. M. S.; Khriachtchev, L.; Fausto, R.; Räsänen, M. *J. Phys. Chem. A* **2004**, *108*, 3380–3389.
- Maçõas, E. M. S.; Fausto, R.; Lundell, J.; Pettersson, M.; Khriachtchev, L.; Räsänen, M. *J. Phys. Chem. A* **2001**, *105*, 3922–3933.
- Maçõas, E. M. S.; Lundell, J.; Pettersson, M.; Khriachtchev, L.; Fausto, R.; Räsänen, M. *J. Mol. Spectrosc.* **2003**, *219*, 70–80.
- Maçõas, E. M. S.; Khriachtchev, L.; Pettersson, M.; Fausto, R.; Räsänen, M. *Phys. Chem. Chem. Phys.* **2005**, *7*, 743–749.
- Dian, B. C.; Longarte, A.; Zwier, T. S. *Science* **2002**, *296*, 2369–2373.
- Clarkson, J. R.; Baquero, E.; Shubert, V. A.; Myshakin, E. M.; Jordan, K. D.; Zwier, T. S. *Science* **2005**, *307*, 1443–1446.
- Nauta, K.; Miller, R. E. *J. Chem. Phys.* **1999**, *111*, 3426–3433.
- Lewerenz, M.; Schilling, B.; Toennies, J. P. *Chem. Phys. Lett.* **1993**, *206*, 381–387.
- Knuth, E. L.; Schilling, B.; Toennies, J. P. *International Symposium on Rarefied Gas Dynamics*; Oxford University Press: New York, 1995; Vol. 19, pp 270–276.
- Harms, J.; Toennies, J. P.; Dalfovo, F. *Phys. Rev. B* **1998**, *58*, 3341–3350.
- Lewerenz, M.; Schilling, B.; Toennies, J. P. *J. Chem. Phys.* **1995**, *102*, 8191–8207.
- Brink, D. M.; Stringari, S. *Z. Phys. D* **1990**, *15*, 257–263.
- Merritt, J. M.; Douberly, G. E.; Miller, R. E. *J. Chem. Phys.* **2004**, *121*, 1309–1316.
- Huang, Z. S.; Jucks, K. W.; Miller, R. E. *J. Chem. Phys.* **1986**, *85*, 3338–3341.
- Nauta, K.; Moore, D. T.; Miller, R. E. *Faraday Discuss.* **1999**, *113*, 261–278.
- Rost, J. M.; Griffin, J. C.; Friedrich, B.; Herschbach, D. R. *Phys. Rev. Lett.* **1992**, *68*, 1299–1301.
- Yang, X.; Kerstel, E. R. T.; Scoles, G. *J. Chem. Phys.* **1993**, *98*, 2727–2741.
- Yang, X.; Kerstel, E. R. T.; Scoles, G. *J. Chem. Phys.* **1993**, *99*, 760–761.
- Nauta, K.; Moore, D. T.; Stiles, P. L.; Miller, R. E. *Science* **2001**, *292*, 481–484.
- Nauta, K.; Miller, R. E. *Chem. Phys. Lett.* **2001**, *346*, 129–134.
- Block, P. A.; Jucks, K. W.; Pedersen, L. G.; Miller, R. E. *Chem. Phys.* **1989**, *139*, 15–30.
- Ewing, G. E. *J. Chem. Phys.* **1979**, *71*, 3143–3144.
- Oudejans, L.; Miller, R. E. *Chem. Phys.* **1998**, *239*, 345–356.
- Oudejans, L.; Miller, R. E. *Annu. Rev. Phys. Chem.* **2001**, *52*, 607–637.
- Lehmann, K. K. *Mol. Phys.* **1999**, *97*, 645–666.
- Stolyarov, D.; Polyakova, E.; Wittig, C. *J. Phys. Chem. A* **2004**, *108*, 9841–9846.
- Nesbitt, D. J.; Field, R. W. *J. Phys. Chem.* **1996**, *100*, 12735–12756.
- Boys, S. F.; Bernardi, F. *Mol. Phys.* **1970**, *19*, 553–566.
- Werner, H. J.; Knowles, P. J.; Almlof, J.; Amos, R. D.; Berning, A.; Deegan, M. J. O.; Eckert, F.; Elbert, S. T.; Hampel, C.; Lindh, R.; Meyer, W.; Nicklass, A.; Peterson, K.; Pitzer, R.; Stone, A. J.; Taylor, P. R.; Mura, M. E.; Pulay, P.; Scheutz, M.; Stoll, H.; Thorsteinsson, T.; Cooper, D. L. *MOLPRO*, version 2002.1, 2002.